Transmetalation Reaction between Hydrophobic Silver Nanoparticles and Aqueous Chloroaurate Ions at the Air−Water Interface

Renu Pasricha, Anita Swami, and Murali Sastry*

Nanoscience Group, Materials Chemistry Division, National Chemical Laboratory, Pune-411 008, India

Received: June 8, 2005; In Final Form: August 1, 2005

The transmetalation reaction between a sacrificial nanoparticle and more noble metal ions in solution has emerged as a novel method for creating unique hollow and bimetallic nanostructures. In this report, we investigate the possibility of carrying out the transmetalation reaction between hydrophobic silver nanoparticles assembled and constrained at the air−water interface and subphase gold ions. We observe that facile reduction of the subphase gold ions by the sacrificial silver nanoparticles occurs resulting in the formation of elongated gold nanostructures that appear to cross-link the sacrificial silver particles. This transmetalation reaction may be modulated by the insertion of an electrostatic barrier in the form of an ionizable lipid monolayer between the silver nanoparticles and the aqueous gold ions that impacts the gold nanoparticle assembly. Transmetalation reactions between nanoparticles constrained into a close-packed structure and appropriate metal ions could lead to a new strategy for metallic cross-linking of nanoparticles and generation of coatings with promising optoelectonic behavior.

Introduction

The synthesis, deposition, and subsequent patterning of thin films of metal nanoparticles is of great interest because of their potential for application as building blocks in nanodevices.[1] It is well-known that metal nanoparticles possess unique optical, chemical, magnetic, and electrical properties, which are different from the properties in their bulk states.[2] Apart from variation in parameters such as size, shape, and dielectric constant of the dispersing medium, these properties can be controlled through their ordered or patterned assembly on suitable substrates.[3] This is because the parameters that influence the collective behavior of assembled nanostructures can now be manipulated by chemists with a high degree of control, thus providing a new initiative to research on cluster-engineered materials. To date, several techniques have been reported for fabricating patterned arrays of nanoparticles on solid surfaces that include spin coating,[4] photolithography,[5] soft lithography,[6] microcontact printing,[7] etc. The Langmuir−Blodgett (LB) technique is a versatile method, which has been extensively used for generating ordered monolayer arrays of metallic,[8] semiconducting,[9] and polymer nanoparticles[10] and their thin film formation. One variant of the LB technique involves spreading a colloidal suspension of hydrophobic nanoparticles on water, allowing the solvent to evaporate, and subsequently transferring the nanoparticle array that forms on the water surface to solid substrates. However, the role of the air−water interface in the above-mentioned cases is relatively passive, since it is utilized merely to organize nanoparticles. An exciting option is to design experiments wherein the air−water interface is dynamic and permits reactions involving nanoparticles. Progress in this direction was made by Chen and co-workers[11] who showed that two-dimensional gold nanoparticle networks could be cross-linked by bifunctional bridging linkers such as TBBT (4,4′-thiobenzenethiol) through hydrogen bonding at the air−water interface. Recently, we have shown in this laboratory how the symmetry-breaking nature of the air−water interface can be exploited to build anisotropic nanostructures by carrying out the reduction of precursor metal ions preferentially at the interface.[12] This has been achieved by either constraining the precursor metal ions (formation of flat gold nanostructures by reduction of a monolayer of hydrophobic gold ions with anthranilic acid in the subphase[12a]) or the reducing agent (formation of flat gold nanosheets by the reduction of gold ions in the subphase by hexadecylaniline[12b]/alkylated tyrosine Langmuir monolayer[12c]) to the air−water interface thus confining the reduction of metal ions strictly to the interface.

In a series of elegant reports, research groups led by Xia[13] and Bai[14] have investigated the possibility of using the transmetalation reaction to modulate the structure of aqueous nanoparticles. The galvanic exchange reaction between sacrificial nanoparticles (which act as a template) and other suitable metal ions often results in the formation of hollow nanostructures[13,14] with interesting application potential. Xia and co-workers have studied in detail the mechanistic aspects of the transmetalation reaction between sacrificial Ag nanospheres/nanocubes and Au ions.[13] They observe that the plasmon absorption band of the metal nanostructures following the replacement reaction can be tuned in the range of 500−1200 nm by simple variation of the experimental conditions.[13] Using Co nanoparticles as sacrificial templates, Bai and co-workers have shown that the transmetalation reaction with Au and Pt ions results in the formation of hollow Pt nanospheres[14a] and rodlike Au−Pt alloy nanoparticles[14b] with excellent catalytic properties.

An interesting possibility that has not been addressed so far is to study transmetalation reactions involving nanoparticles assembled on suitable surfaces/interfaces with appropriate metal ions. An important motivation for such a study is the possibility of interconnecting close-packed nanoparticles assembled on

* To whom correspondence should be addressed. E-mail: m.sastry@ncl.res.in. Current affiliation for Murali Sastry: Chief Scientist, Tata Chemicals Innovation Centre, Mumbai-400 059, India. E-mail: msastry@tatachemicals.com.

10.1021/jp0530552 CCC: $30.25
Published on Web 09/29/2005

surface/interfaces through transmetalation reactions leading to electrically conducting structures over large length scales. That this is indeed a realizable goal is indicated by the rodlike structures observed by Bai et al in the transmetalation reaction of Co nanoparticles and Au/Pt ions; the rodlike structures were explained to arise due to interconnections formed during transmetalation of linearly assembled Co nanoparticles in solution.[14b] In this context, the air−water interface could be an excellent candidate to follow in real time transmetalation reactions between hydrophobic nanoparticles assembled in close-packed structures on water and aqueous metal ions present in the subphase. In this paper, we discuss our experiments on the reaction of aqueous chloroaurate ions in the subphase with hydrophobic silver nanoparticles constrained to the air−water interface. Consumption of the sacrificial silver nanoparticles leads to the formation of gold nanostructures at the air−water interface of interesting morphology. Furthermore, we show that the transmetalation reaction, and thereby the morphology of nanostructures formed at the air−water interface, can be modulated by placing an electrostatic barrier (in the form of Langmuir monolayers of octadecylamine (ODA, cationic) or stearic acid (StA, anionic)) between the hydrophobic silver nanoparticles and the aqueous chloroaurate ions in the subphase. Presented below are the details of the investigation.

Experimental Details

Chemicals. Silver sulfate (Ag_2SO_4), chloroauric acid ($HAuCl_4 \cdot xH_2O$), potassium hydroxide (KOH), tyrosine ($C_9H_{11}NO_3$), stearic acid ($C_{18}H_{36}O_2$), and octadecylamine ($C_{18}H_{39}N$) were obtained from Aldrich Chemicals and used as received.

(a) Synthesis of hydrophobic Silver Nanoparticles. Silver nanoparticles capped with ODA (Ag−ODA) were prepared as described elsewhere.[8d] In a typical experiment, 10 mL of 10^{-3} M aqueous silver sulfate solution was taken along with 10 mL of 10^{-3} M aqueous solution of tyrosine and diluted to 100 mL with deionized water. To this solution, 1 mL of 10^{-1} M solution of KOH was added, and the mixture was allowed to boil until the colorless solution turned yellow, indicating the formation of silver nanoparticles. The aqueous solution of silver nanoparticles (25 mL) was taken in a beaker, and its pH was adjusted to 5 using dilute hydrochloric acid (HCl). This solution was taken in a separating funnel and added to 25 mL of 10^{-3} M solution of ODA in chloroform. Vigorous shaking of the mixture results in the quantitative transfer of silver nanoparticles from the aqueous to chloroform phase. After the completion of phase transfer, the organic phase was separated from the aqueous phase, rotavapped, and washed with ethanol to remove uncoordinated ODA molecules (if any). The purified and dried powder of ODA-capped silver nanoparticles could be dispersed in a range of weakly polar/nonpolar organic solvents.

(b) Transmetalation Reaction of Hydrophobic Silver Nanoparticles with Aqueous Chloroaurate Ions at Air−Water Interface. The transmetalation reaction between ODA-capped silver nanoparticles and aqueous chloroauric acid ($HAuCl_4$) was carried out at the air−water interface using a Nima model 611 LB trough equipped with a Wilhelmy plate as the surface-pressure sensor at room temperature. In a typical experiment, Langmuir monolayers of ODA/StA were formed by spreading a 75 μL solution of ODA/StA in chloroform (1 mg/mL concentration) on the surface of 10^{-3} M aqueous $HAuCl_4$ subphase. At least 15 min was allowed for solvent evaporation, and the monolayer was compressed to a surface pressure of 15 mN/m. An aliquot of 100 μL of Ag−ODA nanoparticle solution in benzene at a concentration of 1 mg/mL was then spread slowly onto the ODA/StA monolayers in a dropwise fashion followed by 15 min of solvent evaporation. At different times in the reaction of the ODA-capped silver nanoparticles with $AuCl_4^-$ ions in the subphase, the nanoparticle monolayers were transferred onto carbon-coated copper grids and quartz slides by the conventional LB method at a controlled surface pressure of 15 mN/m and a substrate immersion/withdrawal speed of 10 mm/min. LB films of Ag−ODA were also formed by nanoparticle organization on deionized water as the subphase under the conditions mentioned above; this serves as a point of reference and a control. The quartz substrates were rendered hydrophobic prior to transfer of the nanoparticles by deposition of three monolayers of lead arachidate onto the substrates. It is known that metal salts of fatty acids (cadmium arachidate, lead arachidate, etc.) form stable monolayers strongly bound to substrates with oxide layers and hydrophobization of the support resulted in significantly better transfer ratios of the nanoparticle monolayers. For the LB films grown on different substrates, monolayer transfer was observed during both upward and downward strokes of the substrate at the close to unity transfer ratio. The transmetalation reaction between silver nanoparticles and gold ions was also carried out by first transferring a thick Ag−ODA LB film on quartz (20 ML) followed by immersion in a 10^{-3} M aqueous $HAuCl_4$ solution.

UV−vis Spectroscopy. The transmetalation reaction between ODA-capped Ag nanoparticles and aqueous gold ions at the air−water interface and in solution was monitored by measuring the UV−vis absorption spectra of LB films of the nanoparticles on quartz substrates at different times of the reaction. The spectra were recorded on a JASCO dual-beam spectrophotometer (model V-570) operated at a resolution of 1 nm.

Transmission Electron Microscopy (TEM). TEM measurements of the Ag−ODA nanoparticles LB films deposited before and after transmetalation reaction at the air−water interface onto carbon-coated copper grids were performed on a JEOL model 1200EX instrument operated at an accelerating voltage at 120 kV. Selected area electron diffraction (SAED) patterns were recorded from ensembles of particles under conditions of an operating voltage of 120 kV, camera length of 80 cm, and insertion of a 120 μm field limiting aperture.

Current−Voltage (I−V) Measurements. The silver nanoparticle film as well as the bimetallic film obtained by transmetalation reaction were deposited onto quartz substrates by vertical lifting and were allowed to dry. After thorough drying, the nanoparticles films were used for I−V measurements. Electrodes of 1 mm width were painted at the opposite ends of the nanoparticulate films using conducting silver paste as thick pads to ensure proper electrical contact. The separation between the electrodes was 10 mm. All I−V measurements were done using a Keithley 238 High Current Source Measure Unit. The I −V characteristics were measured in the sweep mode at a voltage increment of 5 V in the range of −40 to +40 V.

Results and Discussion

Parts A and B of Figure 1 show representative TEM images of a one monolayer (ML) LB film of hydrophobic silver nanoparticles (Ag−ODA) transferred from deionized water as the subphase at a surface pressure of 15 mN/m. It is observed from these images that the hydrophobic silver nanoparticles assemble into large two-dimensional domains of hexagonal close-packed nanoparticles on the surface of water. An analysis

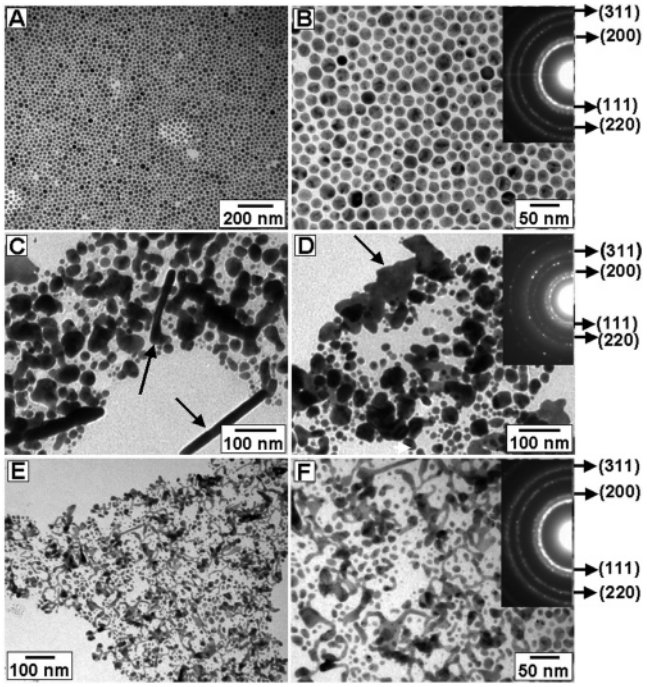

Figure 1. Representative TEM images of one monolayer of ODA-capped silver nanoparticles assembled on deionized water (A and B) and on 10^{-3} M $HAuCl_4$ solution after 1 h of transmetalation reaction with subphase $AuCl_4^-$ ions (C and D). The TEM images in E and F correspond to ODA-capped silver nanoparticles assembled onto the ODA Langmuir monolayer on the surface of 10^{-3} M $HAuCl_4$ recorded after 1 h of reaction. The insets in B, D, and F correspond to SAED patterns recorded from the nanoparticles in the main part of the respective figures.

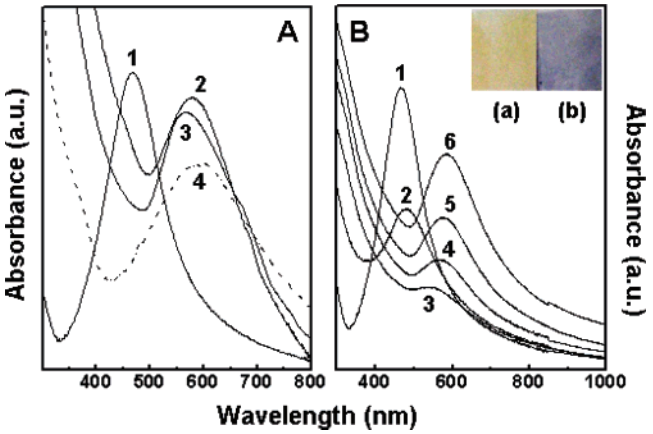

Figure 2. (A) UV−vis absorption spectra recorded from curve 1, 20 ML Ag−ODA LB film from pure water as the subphase and curves 2 and 3, 20 ML LB films of Ag−ODA nanoparticles after 1 h of transmetalation reaction on the surface of 10^{-3} M aqueous $HAuCl_4$ in the presence of StA and ODA monolayers, respectively. Curve 4 corresponds to the UV−vis absorption spectrum recorded from a 20 ML LB film of the Ag−ODA nanoparticles after 1 h of reaction of the nanoparticles with 10^{-3} M $HAuCl_4$ solution in the subphase at the air−water interface. (B) UV−vis absorption spectra recorded from curve 1, 20 ML Ag−ODA LB film from pure water as the subphase (same as curve 1 in Figure 2A) and curves 2−6, 20 ML Ag−ODA LB film deposited from pure water as the subphase after immersion in 10^{-3} M aqueous $HAuCl_4$ solution for t = 10 min, 1, 4, 12, and 48 h, respectively. The inset in the figure shows photographs of a 20 ML Ag−ODA LB film deposited from pure water as the subphase before (a) and after (b) transmetalation reaction by immersion in 10^{-3} M $HAuCl_4$ for 1 h. The pictures correspond to curves 1 and 6 in the figure, respectively.

of the particles in these and other similar images yielded an average nanoparticle size of 20 ± 6 nm. The silver nanoparticles are spherical in nature and often show contrast characteristic of multiply twinned particles (MTPs, Figure 1B). The SAED pattern recorded from the silver nanoparticles is shown as an inset in Figure 1B. The diffraction rings indicate that the particles are polycrystalline and could be indexed on the basis of the face centered cubic (fcc) structure of silver. A 20 ML LB film of the silver nanoparticles was transferred from the water subphase onto a quartz substrate, and the UV−vis absorption spectrum obtained from this film is shown in Figure 2A (curve 1). A strong absorption band centered at ca. 470 nm is observed from the multilayer Ag−ODA film. This absorption is characteristic of excitation of surface plasmon vibrations in the silver nanoparticles and is responsible for the yellow color exhibited by these films (inset of Figure 2B, slide "a"). Well-dispersed silver nanoparticles in water normally show an absorption at ca. 400 nm. The red shift in this absorption band in LB films of the nanoparticles indicates assembly of the nanoparticles[15] or anisotropic nanostructures[16] and also the fact that the dielectric properties of the film are significantly different from those of water. Such shifts have been observed earlier.[15,16] The inference that the particles are in an assembled, close-packed configuration is consistent with the TEM results on monolayers of the Ag−ODA nanoparticles assembled on water (parts A and B of Figure 1).

Parts C and D of Figure 1 correspond to representative TEM images of the Ag−ODA nanoparticle Langmuir monolayer recorded 1 h after reaction with the aqueous $HAuCl_4$ subphase. It is seen that the morphology of the particles has changed dramatically; the original close-packed spherical nanoparticulate structure (parts A and B of Figure 1) is now replaced by irregularly shaped particles that show no ordered packing. Clearly, the transmetalation reaction has taken place, and the irregular structures arise due to consumption of silver nanoparticles by the reduced gold ions. Occasionally, rodlike and triangular structures similar to those observed by us in an earlier study on 4-hexadecylaniline-mediated reduction of gold ions[12b] are seen in the film after transmetalation (structures identified by arrows in part C and D of Figure 1). Further evidence for the occurrence of the transmetalation reaction is provided by the UV−vis spectrum recorded from a 20 ML LB film of the Ag−ODA nanoparticles deposited 1 h after reaction of the nanoparticles with subphase $AuCl_4^-$ ions (curve 4, Figure 2A). The surface plasmon band characteristic of silver nanoparticles (curve 1) is completely damped and is now replaced by an absorption band centered at 588 nm (curve 4). The latter absorption band is a clear indication of the formation of gold nanoparticles by the oxidative reduction of subphase $AuCl_4^-$ ions by the silver nanoparticles. The SAED pattern recorded from the monolayer after the transmetalation reaction is shown as an inset in Figure 1D. The diffraction rings indicate that the particles are polycrystalline and could be indexed on the basis of the fcc structure of gold. We hasten to add here that the crystallography of gold and silver is almost identical, and we rely on the UV−vis data presented above as an indicator that the transmetalation reaction has occurred and that gold has been deposited on the silver structures.

The surface plasmon absorption in spherical, noninteracting gold nanoparticles occurs at ca. 520 nm in water. The shift to longer wavelengths observed in the LB films of the silver nanoparticles post transmetalation is similar to that observed by Xia and co-workers in their study of transmetalation of silver nanocubes by gold ions.[13] The red shift in the gold surface plasmon band was explained as arising due to the formation of

a thin shell of gold around the sacrificial silver nanocube core and under certain experimental conditions, could extend into the near-infrared region of the electromagnetic spectrum.[13] We believe the red shift in the surface plasmon band of gold observed in this experiment may also be explained on the basis of the formation of shells of gold around the spherical silver core, evidence for which will be provided in subsequent studies below. The reaction of subphase chloroaurate ions with the silver nanoparticles at the air−water interface is rapid and is complete within 15 min of spreading the monolayer (data not shown). The silver ions formed as a consequence of the transmetalation reaction are expected to dissolve in the subphase. However, the concentration of the Ag^+ ions was found to be below the detection limits of atomic absorption spectroscopy.

The rate of reaction of subphase gold ions with the silver nanoparticles may be modulated by positioning a suitable barrier between the nanoparticles and the subphase. Since the reaction involves gold ions, an electrostatic barrier comprised of an ionizable lipid monolayer would be an excellent candidate. With this in mind, we have carried out the transmetalation reaction between hydrophobic Ag nanoparticles and $AuCl_4^-$ ions in the subphase in the presence of a cationic (octadecylamine) and an anionic Langmuir monolayer (stearic acid). One would expect that the presence of the cationic ODA monolayer would result in an increase in the $AuCl_4^-$ counterion concentration at the air−water interface and thus, enhance the rate of reaction of the silver nanoparticles with the gold ions. On the other hand, anionic StA would lead to a reduction of $AuCl_4^-$ co-ion concentration at the air−water interface and slow the reaction. Parts E and F of Figure 1 show representative TEM images recorded from the hydrophobic Ag nanoparticle Langmuir monolayer after 1 h of reaction in the presence of an ODA barrier monolayer. The transmetalation reaction in this experiment leads to the formation of a large percentage of elongated and twisted wormlike nanostructures. Clearly, the ODA Langmuir monolayer does not impede the reaction between the gold ions and hydrophobic silver nanoparticles and to a large extent, appears to promote the formation of high aspect ratio nanoparticles most likely due to metallic cross-linking from the transmetalation reaction. The SAED pattern recorded from the monolayer after the transmetalation reaction is shown as an inset in Figure 1F; the diffraction rings could be indexed on the basis of the fcc structure of gold subject to the caveat mentioned earlier.

The UV−vis absorption spectrum recorded from a 20 ML Ag−ODA nanoparticle film transferred after 1 h of reaction with aqueous $AuCl_4^-$ ions in the presence of an ODA Langmuir monolayer barrier is shown as curve 3 in Figure 2A. Complete disappearance of the silver surface plasmon band at 470 nm and appearance of a strong plasmon absorption at 570 nm indicate the completion of the transmetalation reaction and that the elongated structures seen in the TEM images (parts E and F of Figure 1) are due to metallic gold. Attempts were made to follow the kinetics of reaction in this experiment. These experiments (TEM measurements of the silver nanoparticle monolayer at times smaller than 10 min, data not shown) did not show significant differences in the nanoparticle structure at reaction times ~10 min. We note that in these experiments, as well as in those to be described below, the transmetalation reaction between the silver nanoparticle surface and aqueous gold ions takes place even though a hydrophobic sheath of ODA molecules surrounds the particles and in some of the examples, an additional barrier to ion transport in the form of ODA and StA monolayers is present. The galvanic exchange reaction between dodecylthiolate-monolayer-protected Ag clusters and gold ions leading to the formation Ag−Au bimetallic nanoparticles has been reported previously by Murray and co-workers.[17] Taken together with the findings of this study, it is clear that the transmetalation reaction can proceed even in the presence of a barrier to ion transport, the reasons for which need to be elucidated.

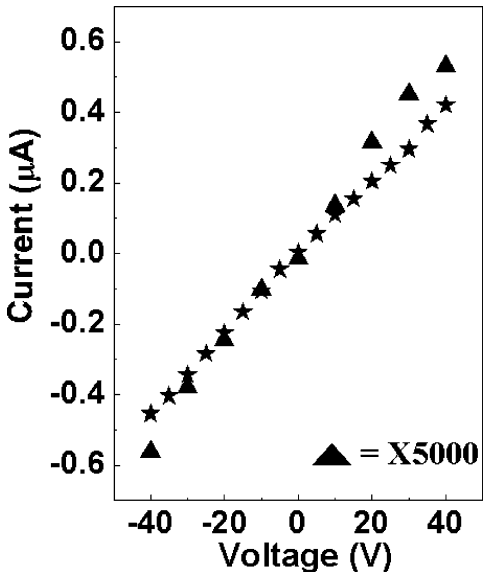

Figure 3. I−V characteristics of 60 ML LB film of silver nanoparticles deposited by vertical lifting on quartz substrate before (triangles) and after (stars) the transmetalation reaction. The current values in the plot obtained before the transmetalation reaction (triangles) have been multiplied by a factor of 5000 to bring the values on the same scale as those recorded from the film after transmetalation (stars).

The TEM images shown in parts E and F of Figure 1 indicate formation of elongated and coiled nanostructures most likely due to metallic cross-linking of the sacrificial silver nanoparticles after the transmetalation reaction in the presence of ODA monolayer; the formation of these interlinked structures was further confirmed by electrical transport measurements. Figure 3 shows the current vs voltage (I−V) plots of a 60 ML LB film of silver nanoparticles before (triangles) and after (stars) the transmetalation reaction. The LB films were deposited on quartz substrates on which the silver electrodes had been deposited by vertical lifting. The I−V plot is fairly linear in both cases, however, the resistance of the film after the transmetalation reaction reduces by an order of 5×10^3 (please note that the current values recorded for the LB film before transmetalation have been multiplied by a factor of 5000 in this plot). The significant drop in the film resistance after transmetalation is a clear indication of the formation of elongated structures leading to an electrical interlinking of the silver nanoparticles observed in the TEM images (parts E and F of Figure 1). The I−V measurements were carried out after thorough drying of the films in a dehumidified atmosphere at different sweep rates and different voltage increments. We did not observe a detectable difference in the I−V plots under these different experimental conditions and believe, therefore, contributions due to water, an so forth, to the electrical conduction may be ruled out. However, more detailed studies are required to fully understand this issue and will be addressed in future communications.

The reaction between subphase gold ions and Ag−ODA nanoparticles in the presence of the anionic Langmuir monolayer, stearic acid, resulted in the formation of structures that were significantly different than those obtained with and without

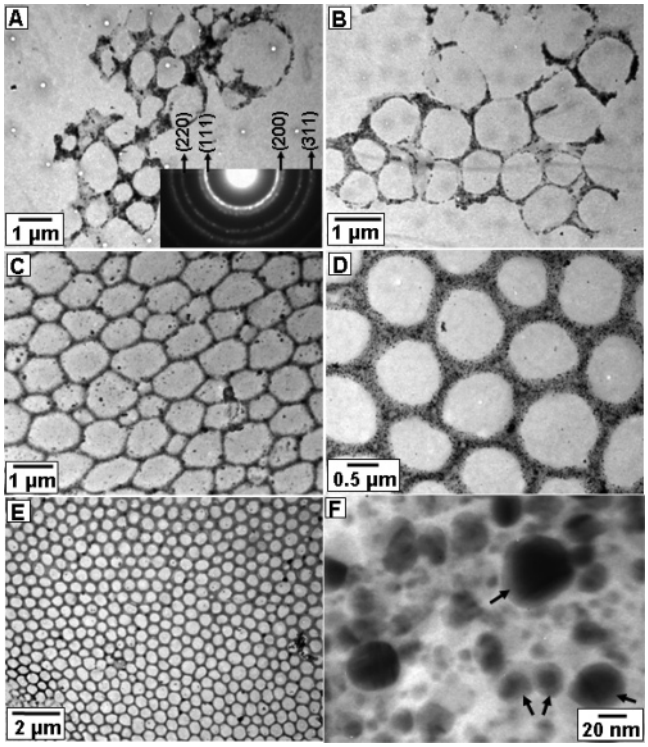

Figure 4. Representative TEM pictures of Ag−ODA nanoparticles as a function of time of the reaction with 10^{-3} M subphase $AuCl_4^-$ ions in the presence of StA as a barrier: A−D, times of reaction t = 15 min, 1, 2, and 3 h, respectively, and E and F, representative TEM images at different magnification recorded from Ag−ODA nanoparticles after 3 h of reaction with subphase $AuCl_4^-$ ions in the presence of the StA barrier.

ODA as a barrier. Due to the slowing down of the reaction for the electrostatic reasons discussed above, the kinetics of reaction could also be followed. Parts A−D of Figure 4 show representative TEM images recorded from the Ag−ODA nanoparticles after 15 min, 1, 2, and 3 h of reaction, respectively, with 10^{-3} M aqueous $HAuCl_4$ in the subphase in the presence of StA as a barrier. It is observed that at the beginning of the reaction, the particles assemble into rudimentary open, ringlike structures (parts A and B of Figure 4) that then close up to form honeycomb-like nanoparticle patterns toward the completion of the reaction (parts C and D of Figure 4). The low and high magnification images of the Ag−ODA nanoparticles after 3 h of reaction illustrate this point better—the honeycomb-like patterns are seen to be composed of nanoparticles of dimensions 10−18 nm along the periphery while the gaps in the structures are devoid of nanoparticles. The assembly of nanoparticles along the periphery of the honeycomb pattern is truly long range and extends well up to 80−100 μm in length. Unlike in the previous cases (reaction of Ag−ODA nanoparticles directly with subphase gold ions and in the presence of ODA Langmuir monolayer), elongated, coiled structures are not seen in this case. The only evidence that the transmetalation reaction has taken place is from the optical properties of a 20 ML LB film of these Ag−ODA nanoparticles transferred onto quartz (curve 2, Figure 2A). The UV−vis absorption spectrum clearly shows a strong absorption band at 578 nm that is characteristic of gold nanoparticles. The SAED pattern recorded from the reacted gold nanoparticles in the presence of StA is shown in the inset of Figure 4A. The ring pattern suggests that the particles are polycrystalline and they could be indexed on the basis of the fcc structure of gold/silver. The fact that the optical properties of the nanoparticles formed by a transmetalation reaction in the presence of ODA (Figure 2A, curve 3) and StA (Figure 2A, curve 2) are rather similar although the structure of the assemblies is so different deserves comment. The similarity in the UV−vis spectra in these experiments suggests that the assembly of the nanoparticles (honeycomb in the case of StA and no regular assembly of ODA barriers) does not play a crucial role in determining the optical properties of the film. In other words, interparticle interaction via plasmon coupling is negligible, and to a large extent, the film properties are determined by the plasmon frequency of the Ag-core−Au-shell bimetallic nanoparticle structure.

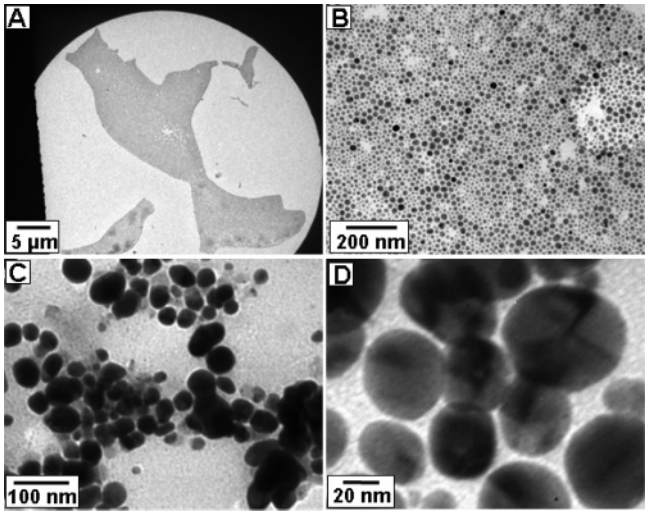

Figure 5. (A and B) Representative TEM images at different magnifications of one monolayer of Ag−ODA recorded 1 h after spreading the monolayer on the surface of pure distilled water (pH adjusted to 3 by diluted HCl) in the presence of StA. (C and D) Representative TEM images of Ag−ODA nanoparticles after reaction with aqueous chloroaurate ions by immersion of a 20 ML Ag−ODA LB film in gold ion solution for 48 h and thereafter dissolved in chloroform.

There could be a number of reasons for the honeycomb structures formed. One is that the transmetalation reaction leads to assembly into such a structure while the second possibility is that there is a separation of the Ag−ODA and StA phases; the transmetalation reaction then proceeds along the Ag−ODA rich phases (which in this case, is the honeycomb pattern). Yet another possibility is that the transmetalation reaction itself drives the phase separation. To test this hypothesis, the Ag−ODA nanoparticles were spread on the surface of deionized water held at pH 3.4 (pH close to that of the 10^{-3} M $HAuCl_4$ solution, pH adjusted using dilute HCl) in the presence of StA and then lifted onto a TEM grid. Parts A and B of Figure 5 show representative TEM images from this monolayer. It is clear that there is no evidence for a honeycomb-structured assembly of the silver nanoparticles and in most respects, the images resemble those recorded from the nanoparticles spread directly onto water (parts A and B of Figure 1). This control indicates that the honeycomb assembly of the nanoparticles is driven by the transmetalation reaction between the silver nanoparticles and the subphase $AuCl_4^-$ ions. The fact that the particles in the honeycomb structures are not interconnected (Figure 4F) suggests that the transmetalation reaction forces the separation of the StA and Ag−ODA phases into the lovely honeycomb pattern observed. Thinking about the possibility of van der Waals or physical interaction between the particles, conductivity measurements were also done for the LB films deposited after transmetalation reaction in the presence of the StA monolayer. However, an increase in the conductivity of

the film was negligible (data not shown for brevity) and nowhere comparable to that obtained in the case of transmetalation in the presence of the ODA monolayer (Figure 3).

It would be of interest to study the transmetalation reaction between LB films of Ag−ODA nanoparticles during immersion in $HAuCl_4$ solution. The UV−vis absorption spectra recorded from a 20 ML LB film of Ag−ODA nanoparticles measured as a function of time of immersion in 10^{-3} M $HAuCl_4$ solution is shown in Figure 2B. It is observed that as the transmetalation reaction proceeds, there is a progressive decrease in the intensity of the silver plasmon band at 470 nm (curve 2, 10 min of reaction) that is then followed by the appearance of a separate and distinct absorption band from metallic gold nanoparticles at ca. 560 nm after 1 h of reaction. Further immersion in the chloroaurate ion solution leads to an increase in the gold plasmon band intensity and a small shift in the peak position to 570 nm (curves 4−6). The reaction is complete after nearly 48 h of reaction and is much slower than the transmetalation reaction between the silver nanoparticles and gold ions at the air−water interface. We believe that this difference in reaction rates is due to the fact that the infusion rate of gold ions and effusion of Ag^+ ions arising from the transmetalation reaction would be much smaller in the case of the LB films of the hydrophobic silver nanoparticles during immersion in chloroauric acid solution. Such a constraint does not occur at the air−water interface where the silver nanoparticles fully access the subphase gold ions with no barrier to metal ion diffusion. The color of this film turned from yellow (inset of Figure 2B, slide "a") to a deep blue upon completion of the reaction with gold ions (inset of Figure 2B, slide "b"). The blue color indicates the interparticle surface plasmon coupling in a monolayer of gold nanoparticles.[15] The 20 ML Ag−ODA LB film after 48 h of immersion in chloroauric acid solution was dissolved in chloroform, and the nanoparticles were imaged by TEM (parts C and D of Figure 5). It is observed that the particles are well separated from one another and that the particles are bigger (average size ∼50 nm) than the as-prepared silver nanoparticles (20 ± 6 nm). This may be attributed to the fact that the AgCl formed after the transmetalation reaction is not able to leach out fully due to entrapment in the lipid monolayer and stays in the form of solid AgCl. We do not observe any interconnection between the nanoparticles possibly because during immersion of the Ag−ODA LB film in the chloroauric acid solution, the film swells and leads to considerable separation between the silver nanoparticles. Transmetalation thereafter may not be capable of interlinking the nanoparticles, and they merely grow in size. We note that the UV−vis absorption curves recorded from the LB films after transmetalation reaction (parts A and B of Figure 2) show the absorbance at ca. 580 nm, indicative of the formation of gold nanostructures. Usually it is observed that the transmetalation reaction between silver nanoparticles and gold ions in either aqueous[13,14] or organic[18] medium leads to the formation of hollow gold nanostructures. However, in the present study, the UV−vis spectroscopy results (parts A and B of Figure 2) indicate the formation of either pure solid gold nanostructures or bimetallic nanostructures (gold-coated silver cores).[19] TEM results support the UV−vis spectroscopy data showing the presence of both solid gold (parts D and F of Figure 1 and Figure 4F) and bimetallic Au−Ag (Figure 4F, particles indicated by arrows) nanostructures. While the exact reasons for this difference are not understood at this moment, we believe the ODA-capping layer surrounding the sacrificial silver nanoparticles may be playing an important role. The ODA monolayer could act as a barrier toward the infusion of $AuCl_4^-$ ions and the effusion of Ag^+ ions during the transmetalation reaction thereby limiting the reaction to the stage where only a thin shell of gold is formed around the silver core. It is known that a gold shell of 3−5 atomic layers is sufficient to dampen the surface plasmon vibrations of the underlying silver core completely[2b,c] and could thus explain the UV−vis spectroscopy trends observed.

In conclusion, we have shown that the facile transmetalation reaction between hydrophobic silver nanoparticles and aqueous chloroaurate ions can be carried out at the air−water interface. Such reactions with nanoparticles assembled into close-packed structures at interfaces could lead to metallic cross-linking of the nanoparticles and synthesis of extended nanoparticulate structures as shown. In the presence of suitable electrostatic barriers, the assembly of the nanoparticles after transmetalation reaction leads to interesting honeycomb-like superstructures. The possibility of connecting nanoparticles in close proximity via electrical contacts shows potential for generation of conducting electrodes with nanoparticles as building blocks and in the design of optical coatings and chemical/biological sensors.

Acknowledgment. A.S. thanks the Council of Scientific and Industrial Research, Government of India, for a research fellowship during the initial stages of this work.

References and Notes

(1) Sastry, M. In *Colloids and Colloid Assemblies: Synthesis, Modification, Organization and Utilization of Colloid Particles*; Caruso, F., Ed.; Wiley-VCH: Berlin, 2003; Chapter 12, p 369. (b) Sastry, M. In *Handbook of Surfaces and Interfaces of Materials*; *Nanostructured Materials, Micelles and Colloids*; Nalwa, H. S., Ed.; Academic Press: London, 2001; Vol. 3, Chapter 2, p 87. (c) Fendler, J. H. *Nanoparticles and Nanostructured Films: Preparation, Characterization and Applications*; Wiley-VCH: Weinheim, Germany, 1998. (d) Rotello, V. *Nanoparticles: Building Blocks for Nanotechnology*; Kluwer Academic/Plenum Publishers: New York, 2004. (e) Horiuchi, S.; Sarwar, M. I.; Nakao, Y. *Adv. Mater.* **2000**, *12*, 1507. (f) Horiuchi, S.; Fujita, T.; Hayakawa, T.; Nakao, Y. *Langmuir* **2003**, *7*, 2963.

(2) El-sayed, M. A. *Acc. Chem. Res.* **2001** *34*, 257. (b) Henglein, A. *J. Phys. Chem.* **1993**, *97*, 5457. (c) Henglein, A. *Chem. Rev.* **1989**, *89*, 1861. (d) Alivisatos, A. P. *J. Phys. Chem.* **1996**, *100*, 13226. (e) Schmid, G. *Clusters and Colloids: From Theory to Application*; VCH: Weinheim, Germany, 1994. (f) Perenboom, J. A. A. J.; Wyder, P.; Meier, P. *Phys. Rep.* **1981**, *78*, 173. (g) Hughes, A. E.; Jain, S. C. *Adv. Phys.* **1979**, *28*, 717.

(3) Andres, R. P.; Bein, T.; Dorogi, M.; Feng, S.; Henderson, J. I.; Kubiak, C. P.; Mahoney, W.; Osifchin, R. G.; Reifenberger, R. *Science* **1996**, *272*, 1323. (b) Kim, S. H.; Medeiros-Ribeiro, G.; Ohlberg, D. A. A.; Williams, R. S.; Heath, J. R. *J. Phys. Chem. B* **1999**, *103*, 10341. (c) Beverly, K. C.; Sampaio, J. F.; Heath, J. R. *J. Phys. Chem. B* **2002**, *106*, 2131. (d) Kim, B.; Tripp, S. L.; Wei, A. *J. Am. Chem. Soc.* **2001**, *123*, 7955.

(4) Xia, D.; Biswas, A.; LI, D.; Brueck, S. R. J. *Adv. Mater.* **2004**, *16*, 1427. (b) Xia, D.; Brueck, S. R. J. *Nano Lett.* **2004**, *4*, 1295.

(5) Lee, K.; Pan, F.; Carroll, G. T.; Turro, N. J.; Koberstein, J. T. *Langmuir* **2004**, *20*, 1812. (b) Horiuchi, S.; Fujita, T.; Hayakawa, T.; Nakao, Y. *Adv. Mater.* **2003**, *15*, 1449.

(6) Xia, Y.; Whitesides, G. M. *Angew. Chem., Int. Ed.* **1998**, *37*, 550. (b) Gorman, C. B.; Beibuyck, H. A.; Whitesides, G. M. *Chem. Mater.* **1995**, *7*, 526. (c) Zhao, X. M.; Xia, Y.; Whitesides, G. M. *J. Mater. Chem.* **1997**, *7*, 1069.

(7) Santhanam V.; Andres, R. P. *Nano Lett.* **2004**, *4*, 41.

(8) Sastry, M.; Patil, V.; Mayya, K. S.; Paranjape, D. V.; Singh, P.; Sainkar, S. R. *Thin Solid Films* **1998**, *324*, 239. (b) Perez, H.; Lisboa de Sousa, R. M.; Pradeau, J. P.; Albouy, P. A. *Chem. Mater.* **2001**, *13*, 1512. (c) Swami, A.; Kumar, A.; Selvakannan, PR.; Mandal, S.; Sastry, M. *J. Colloid Interface Sci.* **2003**, *260*, 367. (d) Selvakannan, PR.; Swami, A.; Srisathiyanarayanan, D.; Shirude, P. S.; Pasricha, R.; Mandale, A. B.; Sastry, M. *Langmuir* **2004**, *20*, 7829. (e) Wang, W.; Chen, X.; Efrima, S. *J. Phys. Chem. B* **1999**, *103*, 7238. (f) Heath, J. R.; Knobler, C. M.; Leff, D. V. *J. Phys. Chem. B* **1997**, *101*, 189. (g) Burghard, M.; Philipp, G.; Roth, S.; von Klitzing, K.; Pugin, R.; Schmid, G. *Adv. Mater.* **1998**, *10*, 842. (h) Bourgoin, J. F.; Kergueris, C.; Lefevre, E.; Palacin, S. *Thin Solid Films* **1998**, *327−329*, 515. (i) Chen, X. Y.; Li, J. R.; Jiang, L. *Nanotechnology*

2000, *11*, 108. (j) Brust, M.; Stuhr-Hansen, N.; Nørgaard, K.; Christensen, J. B.; Nielsen, L. K.; Bjørnholm, T. *Nano Lett.* **2001**, *1*, 189. (k) Brown, J. J.; Porter, J. A.; Daghlian, C. P.; Gibson, U. J. *Langmuir* **2001**. (l) Huang, S.; Minami, K.; Sakaue, H.; Shingubara, S.; Takahagi, T. *Langmuir* **2004**, *20*, 2274.

(9) Kotov, N. A.; Meldrum, F. C.; Wu, C.; Fendler, J. H. *J. Phys. Chem.* **1994**, *98*, 2735. (b) Tian, Y.; Fendler, J. H. *Chem. Mater.* **1996**, *8*, 969. (c) Damle, C.; Gole, A.; Sastry, M. *J. Mater. Chem.* **2000**, *10*, 1389.

(10) Lennox, R. B.; Goren, M. *Nano Lett.* **2001**, *1*, 735. (b) Seo, Y. S.; Kim, K. S.; Galambos, A.; Lammertink, R. G. H.; Vancso, G. J.; Sokolov, J.; Rafailovich, M. *Nano Lett.* **2004**, *4*, 483. (c) Yoo, S.; Sohn, B. H.; Zin, W. C.; Jung, J. C. *Langmuir* **2004**, *20*, 10734.

(11) Chen, S. *Adv. Mater.* **2000**, *12*, 186. (b) Chen, S. *Langmuir* **2001**, *17*, 2878.

(12) Swami, A.; Kasture, M.; Pasricha, R.; Sastry, M. *J. Mater. Chem.* **2004**, *14*, 709. (b) Swami, A.; Kumar, A.; Selvakannan, PR.; Mandal, S.; Pasricha, R.; Sastry, M. *Chem. Mater.* **2003**, *15*, 17. (c) D'Costa, M.; Pasricha, R.; Sastry, M. *J. Mater. Chem.* **2004**, *14*, 2696.

(13) Sun, Y.; Mayers, B.; Xia, Y. *Adv. Mater.* **2003**, *15*, 641. (b) Sun, Y.; Xia, Y. *J. Am. Chem. Soc.* **2004**, *126*, 3892. (c) Sun, Y.; Mayers, B. T.; Xia, Y. *Nano Lett.* **2002**, *2*, 481.

(14) Liang, H.; Zhang, H.; Hu, J.; Guo, Y.; Wan, L.; Bai, C. A*ngew. Chem., Int. Ed.* **2004**, *43*, 1540. (b) Liang, H. P.; Guo, Y. G.; Zhang, H. M.; Hu, J. S.; Wan, L. J.; Bai, C. L. *Chem. Commun*. **2004**, 1496.

(15) Sastry, M.; Patil, V.; Sainkar, S. R. *J. Phys. Chem. B* **1998**, *102*, 1404. (b) Swami, A.; Selvakannan, PR.; Pasricha, R.; Sastry, M. *J. Phys. Chem. B* **2004**, *108*, 19269. (c) Zhao, L.; Kelly, K. L.; Schatz, G. C. *J. Phys. Chem. B* **2003**, *107*, 7343. (d) Haynes, C. L.; McFarland, A. D.; Zhao, L.; Van Duyne, R. P.; Schatz, G. C. *J. Phys. Chem. B* **2003**, *107*, 7337. (e) Bouhelier, A.; Bachelot, R.; Im, J. S.; Wiederrecht, G. P.; Lerondel, G.; Kostcheev, S.; Royer, P. *J. Phys. Chem. B* **2005**, *109*, 3195.

(16) Hao, E.; Kelly, K. L.; Hupp, J. T.; Schatz, G. C. *J. Am. Chem. Soc.* **2002**, *124*, 15182. (b) Kelly, K. L.; Coronado, E.; Zhao, L. L.; Schatz, G. C. *J. Phys. Chem. B* **2003**, *107*, 668. (c) Hao, E.; Bailey, R. C.; Schatz, G. C.; Hupp, J. T.; Li S. *Nano Lett.* **2004**, *4*, 327. (d) Me'traux, G. S.; Cao, Y. C.; Jin, R.; Mirkin, C. A. *Nano Lett.* **2003**, *3*, 519.

(17) Shon, Y.-S.; Dawson, G. B.; Porter, M.; Murray, R. W. *Langmuir* **2002**, *18*, 3880.

(18) Selvakannan, P. R.; Sastry, M. *Chem Commun.* **2005**, 1684.

(19) Link, S.; Wang, Z. I.; El-Sayed, M. A. *J. Phys. Chem. B* **1999**, *103*, 3529.